sustainability

MDPI

Article

An Active Drying Sensor to Drive Dairy Cow Sprinkling Cooling Systems

Paolo Liberati

Department of Agricultural and Food Sciences, Alma Mater Studiorum, University of Bologna, 40126 Bologna, Italy; paolo.liberati@unibo.it

Abstract: The use of sprinkling with ventilation to cool dairy cows is considered an appropriate practice to reduce the negative effects of heat stress. However, due to climate change, water will increasingly become a limited resource, so we need to make water use more and more efficient. For this purpose, an active drying sensor has been developed in order to time the sprinkling cooling system. The sensor reproduces the thermal response of a cow, considering both sensible and latent heat exchange, and is located in the feeding alley, about two meters above the floor. This allows the fabric of the sensor (simulating the fur) to be wetted by the sprinkler, and blown by the fan. The water content of the sensor fabric during the drying time is monitored by measuring its electrical conductivity, allowing the estimation of the time the fur becomes dry. Another two specifically designed instruments are presented, the first to estimate the fur's water content after spraying, and the second to detect the time the fur became dry. Sensor output, interpreted through a simplified model, gave a predicted drying time with an error ranging between −11.4% and +14.8% (R^2 = 0.789). In the commercial barn where the experiments were conducted, the use of the sensor allowed an estimated reduction in water consumption of about 57%, with respect to the fixed timing normally used. As a perspective, the sensor could be used to assess cows' heat stress level.

Keywords: dairy cow; active sensor; water consumption; heat stress; heat and mass transfer; evaporative cooling

Citation: Liberati, P. An Active Drying Sensor to Drive Dairy Cow Sprinkling Cooling Systems. *Sustainability* **2023**, *15*, 9384. https://doi.org/10.3390/su15129384

Academic Editor: Pablo Rodríguez-Gonzálvez

Received: 29 April 2023
Revised: 31 May 2023
Accepted: 7 June 2023
Published: 10 June 2023

1. Introduction

Climate change makes mitigation actions necessary to ensure the adequate conditions of the animals bred due to the increasingly hot microclimate. In dairy cow breeding, coordinated water spraying and fan airflow targeting the animals are used to reduce heat load ('sprinkling cooling system'), among other available systems [1–3], as ascertained by various authors [4–6]. In these cooling systems, spray/fan timing is fixed, although there are some attempts to link it, on an empirical basis, to the THI, or to other more- or less-simplified models [7].

In particular, in [7], several models to predict the dairy cow's thermal state using several approaches such as bioclimatic indexes, machine learning or mechanistic modelling are reviewed [7]. In a recent work, Shu et al. [8] tested several algorithms through machine learning, and stated that ANN gives the lower error in predicting the physiological responses of dairy cows, allowing a better cooldown decision.

To optimise water and energy consumption, the sprinkling should take place just before the water deposited in the previous spraying on the fur of the cow has completely evaporated—not after, not before. Some researchers have modelled the behaviour of heat exchange with stationary models [9,10], also considering latent heat exchange, without giving any indication of the drying time of the fur. Chen et al. in [11] improved previous works by developing a transient model to predict the drying time of the fur under varying conditions. They also presented a parametric algorithm to directly control a cooling system. In this work, assumptions of some parameters are somewhat uncertain, for example, the fur water content after showering was derived backwards from the findings of other authors.

Other works evaluated the heat exchange characteristics of the fur [12]. Although the use of sprinkling with ventilation is considered an appropriate practice to reduce heat stress, there are several critical operational aspects to this methodology, such as the flow rate of the sprayer or the duration of shower/water delivery [12]. Some authors have pointed out that even with low flow rates (1.5 L min^{-1} $sprayer^{-1}$), a shower of 30/60 s may be sufficient to adequately wet the cow's fur [10,13]. Authors adopted an empirical approach to determine the wetting time, identified as the time the water begins to run off from the abdomen. The same authors warn about the need to avoid wetting the udder to prevent mastitis cases. Due to these reasons, the research did not propose any models to simulate the wetting phase. In fact, Chen et al. [11], in predicting the wetting phase, declared that it occurs in a few seconds.

Obviously, the diameter distribution of sprinkler droplets also influences wetting, although coarse droplets are preferred to smaller ones as they wet the fur deeper [14–17]. In any case, in Arkin et al. [12] it is reported that fur wets at only 60 percent of the fur's maximum capacity with normal commercial sprinklers. On the other hand, one aspect considered important enough to be investigated is the duration of the wetting/ventilation cycle as it determines the number of daily showers and, then, given the sprinkler's flow, global water consumption.

Bouy et al. [1] gave recommendations to improve the performance of PLF to determine heat stress and the response of animals to various environmental conditions. Then, as water will increasingly become a limited resource [16], it is desirable to have a sensor to guide the actuation of the nozzles in order to optimise water efficiency.

Most of the models analyzed in [7] assess the thermal behaviour of animals, but they do not address the estimation of the fur's drying time, apart from Chen et al. [11]. Shu et al. [8], on the other hand, assess the response of cows to the cooling treatment only afterwards, through different predictors of physiological states. Furthermore, most modelling approaches use ambient parameters (Ta, RH) which remain almost unchanged, even after sprinkler activation (apart from a possible increase in RH), which acts on the animal and does not appreciably change the Ta and RH of the ambient air. Therefore, models relying on Ta and RH could continue to indicate a state of stress. Such models, therefore, may be adequate enough to determine when cooling should be performed, but they are not adequate enough to manage the strategy of the cooling system (sprinkler/fan activation timing) apart from, as mentioned above, the model proposed by Chen et al. [11].

In the present work, an active drying sensor, to be installed in the feeding alley, to emulate cow heat exchange(sensible and latent), cow heat production, and the wetting/drying dynamics of the cow's coat, thus giving information on the evolution of the drying process and allowing the timing of the sprinkling cooling system (fan velocity, sprinkling timing, etc.) to be managed, was evaluated.

The sensor proposed herein could also be used to assess the heat stress state of the animals, but this aspect was not yet investigated in the present work.

The sensor was evaluated both in a laboratory and in a commercial dairy cow barn equipped with its own cooling system.

2. Materials and Methods

2.1. The Experimental Barn

The commercial barn where the experimentation was carried out houses 110 lactating Holstein cows in a cubicle system. Mean daily milk yield was 29.5 kg d^{-1} $head^{-1}$. The field tests were conducted in August 2022.

The barn was equipped with a sprinkling cooling system; showers were arranged 2 m above the feeding alley and 2 m apart. The water flow rate was 1.4 L min^{-1}.The treatment scheme used was nominally 60 s of shower (de facto 67 s) and 300 s of fan; when the shower was on, the fan ran at 10% of its full speed.

Since in the experimentation fur drying was not achieved within 300 s of wetting, the sprinkler near the tested cows was disabled to allow the cows' fur to fully dry; with this scheme, the sprinkler/fan timing was 1 min/17 min.

2.2. The Drying Sensor

The drying sensor is an active device acting to simulate cow heat dissipation also considering the contributions of wetted fur. The sensor has been designed to be installed in the manger alley (Figure 1).

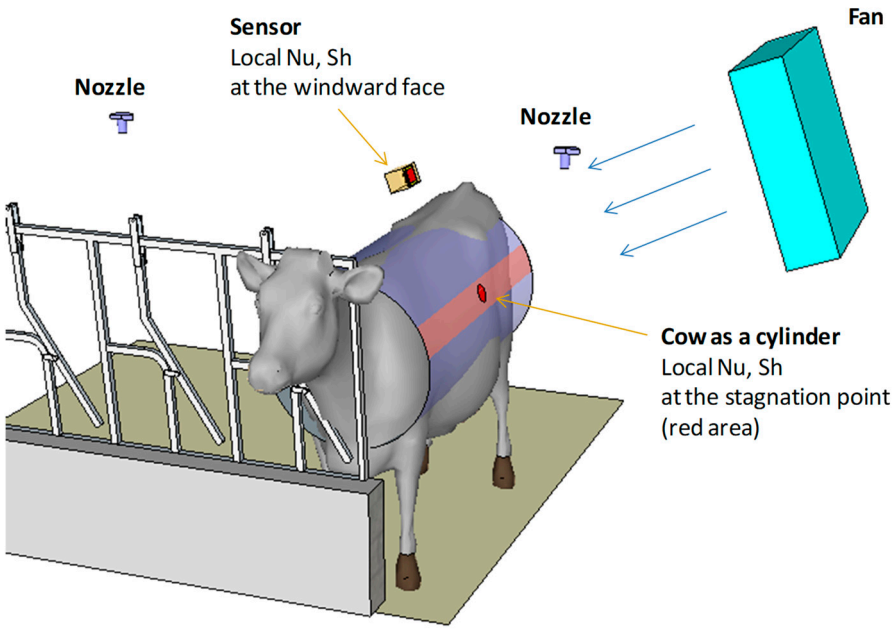

Figure 1. Layout of the experimental facility. Cows are locked to the self-locking head rails during the test. Measurements on the cows(saturation fur wetness (at the end of the shower), fur IR temperature and fur EC (during draying)) were made in the area close to the stagnation point (pink strip area), while the sensor was on the downwind face, where the fabric was located.

The sensor consists of three layers (Figure 2): the innermost consists of an aluminum plate (thickness = 0.0005 m) maintained at the cow's core body temperature of 38.7 °C [11,18] by two ceramic-encased heating resistor elements, which were controlled by a purposely designed control system.

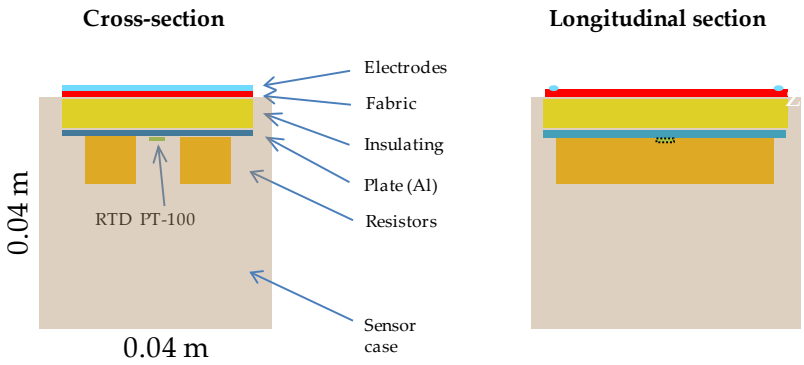

Figure 2. Sections of the sensor (not in scale): Resistors = heating elements, RTD PT-100 = temperature sensor, Plate = aluminum plate (thickness = 0.5 mm), PTFE insulation layer (2.7 mm), Fabric (35 × 30 mm), and Electrodes = stainless steel electrodes. The temperature sensor gives feedback to the resistor control system to maintain the aluminum plate at 38.7 °C.

A PTFE insulation (second layer) was placed over the aluminum plate to represent the tissue resistance of the cow.

In place of the fur, a third layer of cotton fabric was placed over the insulation. The fabric was fastened by two stainless steel electrodes at their shorter ends, to allow the measurement of the electrical conductivity (EC) of the fabric during drying, after being wetted by the action of the sprinkling (Figure 2).This allowed for the estimation of the residual water content, and thus the prediction of the drying state of the fabric itself. The residual water content (RWC_t) is calculated by the following equation:

$$RWC_t = WC_{max} (1 - EC_t/EC_{max}) \quad (1)$$

where WC_{max}, EC_{max} = the maximum water content and EC of the fabric at the end of spraying, respectively; and EC_t = EC during drying.

A thermal conductive compound was used between the ceramic heating elements and the aluminum plate, and between the aluminum plate and the insulation layer to improve heat transfer; the compound was also used in the junction between the plate and the RTD PT100 sensor.

The resistance of the insulation was also verified through the sensor's power balance (Equation (2)). The insulation showed a thermal conductivity of λ = 0.20 W m^{-1} K^{-1} (comparable to the values found in the literature of 0.23–0.25 W m^{-1} K^{-1})which, for a thickness of 0.0027 m, results in a thermal resistance of 0.0135 m^2 K W^{-1}. Such resistance is about 4.3 times lower than that used by Chen et al. [11], and by other authors to represent the cow tissue's resistance (R_{tissue} = 0.0585 m^2 K W^{-1}).

To relate the behavior of the sensor to the drying fur, we need to know the time the fur become dry, and the water content of the fur after the shower. For this reason, a hand-held fur conductivity probe(Section 2.3), and a field method to assess the fur water content by dubbing (Section 2.5) were developed.

2.3. The Hand-Held Fur Conductivity Probe

To evaluate the complete drying of the fur, Tresoldi et al. [14] used a cobalt-chloride-embedded paper to estimate when the fur became dry.

In the current work, the electrical conductivity of the fur was measured. The hand-held conductivity probe (Figure 3), specially designed, consists of two electrodes, which are pressed against the fur when measurement is performed. To exert controlled pressure and improve the repeatability of the measurement, the electrodes are retractable by a spring, with a pressure of about 7.6 N cm^{-2}.

During the development of the device, stray currents were detected on the cow due to various unidentified causes; consequently, a capacitor to block the DC component distorting the EC measurements was added (Figure 4).

2.4. Measuring Circuit of Electrical Conductivity of the Wetted Fabric and Fur

By measuring the electrical conductivity of the wetted fabric, the degree of saturation was evaluated and, thus, the amount of residual water present in the fabric itself was also evaluated.

The measurement circuit works with an alternating square wave current, obtained by two counter-phase oscillating digital outputs (D1, D2, Figure 4) at 3125 Hz. Frequency does not affect EC measurement within a wide tested range (450–4500 Hz). The acquired EC was the average of 30 readings.

The circuits were calibrated with and without the capacitor, yielding two separate calibration functions, respectively, for the hand EC fur probe, and the EC fabric electrodes of the sensor.

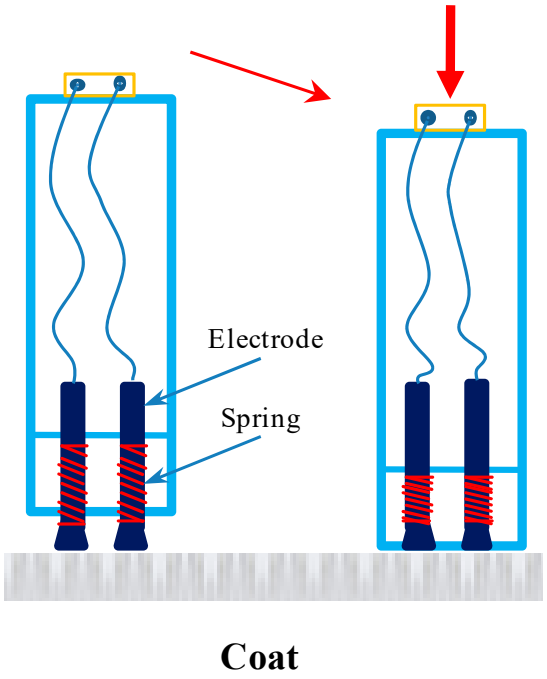

Figure 3. Hand probe to measure the fur's electrical conductivity in order to evaluate the drying process of the coat. The sensor is designed to allow the regular pressure of the electrode on the fur to improve the repeatability of measurement. The probe is connected to the circuit of Figure 4, in place of the fabric electrodes.

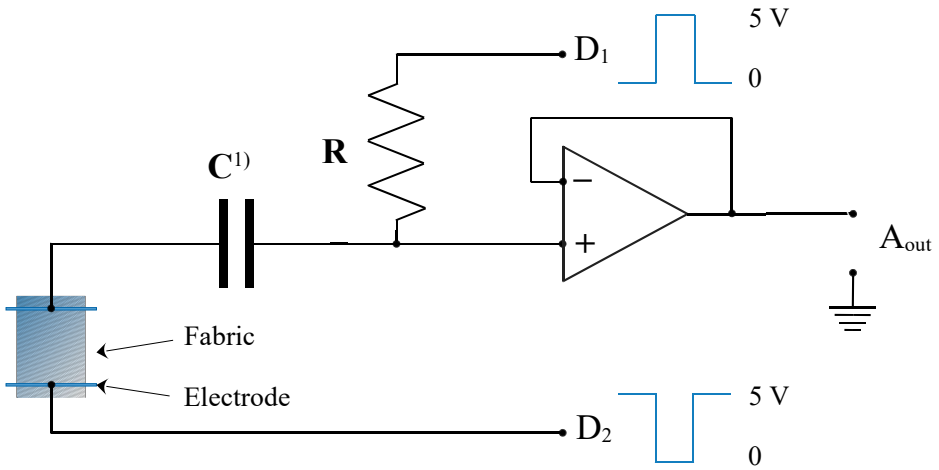

Figure 4. Schematic of the measuring circuit of electrical conductivity of the fabric/fur. The signal A_{out} represents the analog output, proportional to EC. [1)] The configuration with the capacitor is the circuit used by the EC hand probe for the evaluation of the drying state of fur, with the cow at the manger (see Section 2.3).

2.5. In-Field Evaluation of the Water Content of the Wetted Fur after Shower

A method was developed to estimate the water content in fur wetted by showers. A 16 cm^2 area of saturated fur, bounded by a mask set on the coat (Figure 5), was vigorously dabbed repeatedly with three pieces of fabric. A fourth dabbing fabric did not improve the final accuracy of the fur water content estimation.

Figure 5. Mask placed on the fur that was used to delimit the area to be dabbed (16 cm^2), to evaluate the fur's water content after shower.

An initial estimate of the accuracy was evaluated by lab tests with an excised fur; after dabbing, some water was remained in the fur's internal structure in an almost fixed amount (24.8 $gm^{-2} \pm 4.1$ g m^{-2}, M ± SD). This means that by using the described method, the error will be smaller than if done on saturated or quasi-saturated fur, which is the case for our estimations (the error was about 9.6%). In any case, the remained fixed amount was added to the quantity of water found by dabbing.

2.6. Instrumentation Used

The sensor is controlled by computer software specifically developed for the present work. It continuously acquired the following: (1) air temperature and air RH (by HTU21D RH/Ta sensor produced by TE Connectivity company (Schaffhausen, Switzerland); Accuracy: RH ± 2%, Ta ± 0.3 °C); (2) the fabric's electrical conductivity; (3) the aluminum plate's temperature (T_{Bs}); and (4) the hand probe's measurements of the electrical conductivity of the fur, when applied.

The control system allowed the plate temperature to be constant at the defined value (T_{Bs} = 38.7 °C) by controlling the activation of the heating elements according to the temperature of the aluminum plate.

Finally, the control software used for the experimentation allowed for observations to be entered into the log file, which was very useful when inputting fur/fabric spot temperatures measured by the infrared thermometer, and when adding comments to in-field and in-lab experimentation.

Spot measurements were made for air velocity with a hot-wire anemometer (Delta Ohm, model HD9216, Caselle di Selvazzano, Italy), and also for air temperature and humidity (Testo, model 425, Titisee-Neustadt, Germany).

2.7. IR Thermometer vs. Thermocouple Measurements

To measure surface temperature of the fur/fabric during drying, an IR thermometer was used (Fluke 561 HVAC Pro, Everett, WA, USA).To verify the response of the IR thermometer in the presence of water, both on fur and fabric, the surface temperature was compared with a type-K thermocouple measurement.

The difference was about 0.5 °C (infrared > thermocouple), both on white and black fur, with the Fluke IR thermometer set with $\varepsilon = 0.95$.

Gonçalves et al. [19] showed that different porous materials wetted with water have similar emissivity (Mean = 0.95, SD = 0.2); so, we can assume that we are doing the measurement accurately by setting the IR thermometer with $\varepsilon = 0.95$.

2.8. Theoretical Assumptions

The sensor works with transverse flow, as this condition allows the highest evaporation rate, that is, the shortest drying time (with respect to the parallel flow. At the theoretical level and during field tests, the comparison between the fur and the sensor was done by considering the local Nusselt number and the local Sherwood number, modelling the cow as a cylinder (Figure 1), as the aptly-named cow-cyl (diameter of the cylinder, D = 0.8 m [11]).

The local Nusselt number for the cow-cyl was calculated at the stagnation point (around the pink strip area in Figure 1), obtained by tabulating and interpolating the curves of the graph in [20] (Figure 7.9) as a function of the Re number (valid for $Re = 24 \times 10^3 - 200 \times 10^3$; $v_a = 0.5–4$ m s^{-1}).

To calculate the local Nusselt number, considering only the downwind face of the sensor (Figure 1), a square cylinder configuration was considered, using data from Abd-Rabbo et al. [21] (Figure 10), which was handled the same as in cow-cyl (valid for $Re \approx 2.2 \times 10^3 - 9.8 \times 10^3$; $v_a = 0.9–4$ m s^{-1}).

The sensor obviously had no geometrical or dynamic similarity when compared to the cow-cyl; so, the output of the sensor has to be interpreted to relate it to the behavior of the drying fur of the cow.

2.9. A Simplified Physical Model to Estimate Fur Drying Time from Sensor Output

Referring to the model proposed by Gebremedhin and Wu [10], neglecting radiant heat exchange, a code was developed to solve, by iteration, the surface temperature (Ts_s) of the drying surface of the sensor, considering the power balance (Figure 6):

$$Q_S = Q_c + Q_{evap} \quad (2)$$

where Q_s is the total heat loss of the sensor (W m^{-2}), Q_c is the convective heat flow (W m^{-2}), and Q_{evap} is the latent heat flow (W m^{-2}).

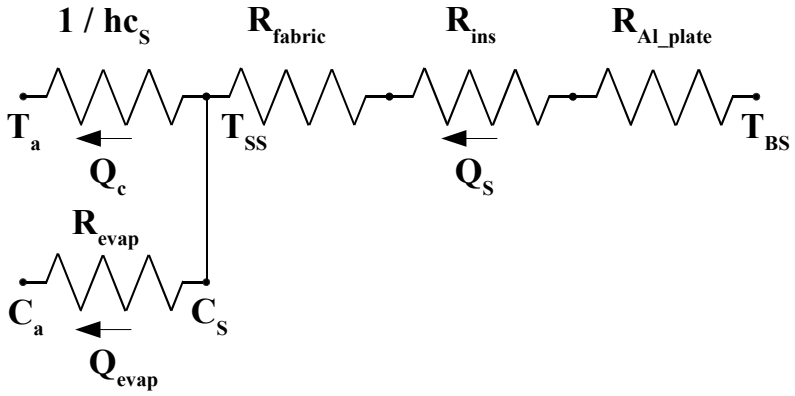

Figure 6. Thermal-electrical analogy of the sensor: hc_s = convection coefficient, R_{fabric} = resistance of the fabric layer, R_{ins} = resistance of the insulation layer, R_{Al_plate} = resistance of the aluminum plate, C_a and C_s = molar concentration, $Q_{evap} = (C_s - C_a)/R_{evap}$, $R_{evap} = 1/(hm_s \cdot MW_w \cdot J)$ (m W kmol^{-1}); and hm_s = convective mass transfer coefficient (m s^{-1}).

That is:

$$(T_{Bs} - Ts_s)/R_{ins} = hc_s\,(Ts_s - Ta) + Wa_s \cdot J \quad (3)$$

where R_{ins}(K m^2 W^{-1}) is the resistance of the insulation layer, T_{Bs} represents the core (body) temperature of the sensor (set to 38.7 °C), Ts_s is the surface temperature (°C), T_a is the air temperature (°C), Wa_s is the rate of evaporation of water from the fabric (kg m^{-2} s^{-1}), and J is the latent heat of evaporation of water (J kg^{-1}).

The thermal resistances of aluminum (R_{Al_plate}) and fabric (R_{fabric}) were not considered in calculating Qs because their contribution to the global resistance can be considered negligible for the purposes of the simplified model of Equation (3).

Wa_s is obtained by applying Equation (1) to two points of the drying process:

$$Wa_s = (RWC_{t1} - RWC_{t0})/(t_1 - t_0) \quad (4)$$

where t_0 represents the beginning time of the drying process, while t_1 can be updated as the drying progresses, allowing a mean Wa_s for a longer period.

When T_{Ss} was obtained (i.e., the condition of Equation (2) is achieved), the boundary conditions of the sensor were reconstructed, and thus the convective mass transfer coefficient (hm_s, m s^{-1}) was determined, then the Sherwood number (Sh_s), from which the local Nu_s number for the sensor was calculated, and consequently the convective coefficient of the sensor (hc_s). This allowed the evaluation of Equation (2) at each iteration. For details, see Appendix A.

From Nu_s, in the backward direction, Re_s was calculated and, finally, so too was v_a. Knowing the v_a enabled the derivation of the local Nu $_{cow\text{-}cyl}$ number and then hc $_{cow\text{-}cyl}$, and the air velocity v_a (m s^{-1}) of the fan.

Assuming that Ts_s approximates $Ts_{cow\text{-}cyl}$, and rearranging Equation (3) for the cow, solving for $Wa_{cow\text{-}cyl}$ obtains the rate of evaporation of the fur:

$$Wa_{cow\text{-}cyl} = (T_{Bcow\text{-}cyl} - Ts_{cow\text{-}cyl})/(R_{tissue} \times J) - hc_{cow\text{-}cyl}\,(Ts_{cow\text{-}cyl} - T_a)/J \text{ (kg m}^{-2}\text{ s}^{-1}\text{)} \quad (5)$$

where $T_{Bcow\text{-}cyl}$ is the core body temperature of the cow, $hc_{cow\text{-}cyl}$ (W m^{-2} K^{-1}) is the convective heat coefficient of the cow-cyl, and $Ts_{cow\text{-}cyl}$ is the surface temperature of the cow.

At this point, knowing the initial water content of the fur ($W_{fur\ sat}$, kg m^{-2}), determined as per Section 2.5, the drying time (t_{dry}) was calculated as follows:

$$t_{dry} = Wa_{cow\text{-}cyl}/W_{fur\ sat} \text{ (s)} \quad (6)$$

2.10. Theoretical Comparison of the Thermal Response of Cow and Sensor—Sensitivity Analysis

Although the sensor has no similarity with the cow-cyl, by applying the model, as in Equation (3), to the sensor and to the cow, responses were compared from the thermal point of view for two temperatures (27 and 32 °C), and for two v_a (1.0 and 3.0 m s^{-1}), while RH was 40% for all simulations. The following heat ratios were compared: Q_c/Q_s, Q_c/Q_{evap}, and Q_s/Q_{evap}

The tissue and sensor resistances in the simulations were set, respectively, to R_{tissue} = 0.0585, and R_{ins} = 0.0135 (R_{tissue}/R_{ins} = 4.3).

Sensitivity analysis was carried out referring to the model by applying Equation (3) to calculate $Wa_{cow\text{-}cyl}$. The reference model conditions were: $Ts_{cow\text{-}cyl}$ = 25 °C, $hc_{cow\text{-}cyl}$ = 16 W m^{-2} K^{-1}, and Ta = 32 °C. The introduced error for $Ts_{cow\text{-}cyl}$ was ranging from 2% to 14%, while for $hc_{cow\text{-}cyl}$, the introduced error was higher as its variation affects Wa less, ranging from 10% to 70%.

3. Results and Discussion

3.1. Evaluation of Water Content of the Fur after Shower

The water content of the saturated fur after shower was evaluated in the cowshed in April and August by the dabbing method, as described in Section 2.5.

In the period with lower ambient temperature (April), the water contained in the hair after showering was higher than in the summer period (August), measuring at 408.2 ± 38.6 and 213.4 ± 10.6 (M ± SD, g m^{-2}), respectively. The differences were due to the environmental temperatures (still cold in April), and the subsequently thicker and longer hair coat (with respect to August).

Arkin et al. [12] stated that the maximum fur water content "was some 230 g m^{-2}" by means of a commercial sprinkler. The boundary conditions (degree of wetness of the fur and fan air speed) resulting from the cow-sprinkler-fan system were highly variable depending on the relative position of the cow on the self-locking headrails with respect to the sprinkler and fan locations.

In the present work, a mean condition regarding the distance of the cow from the fan was assumed, together with the minimum saturation of the August period.

3.2. Sensor Behaviour

The graphs in Figure 7 were obtained using the sensor in laboratory tests. The graph of Figure 7a was obtained by wetting the fabric already assembled with the sensor, while Figure 7b shows the EC of the fabric saturated outside the sensor, and then assembled with it for the drying process.

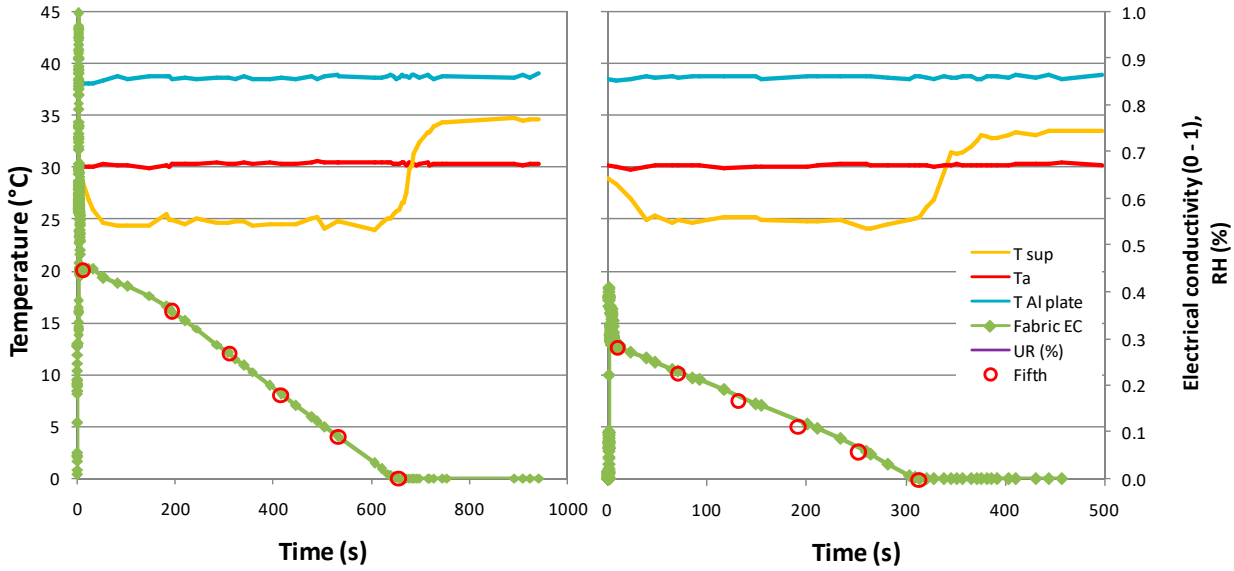

Figure 7. Sensor fabric in the laboratory drying process: (**a**) wetting with the fabric already assembled with the sensor (273.84 g m^{-2}, drying time = 650 s); (**b**) wetting with the fabric disassembled and softly shaken, and then inserted into the sensor (138.87 gm^{-2}, drying time = 703 s). Wa_a = 0.421 g $s^{-1}m^{-2}$, Wa_b = 0.432 g s^{-1} m^{-2} and difference $Wa_{a/b}$ = −2.5%. Environmental test conditions: T_a = 30.1 °C, RH = 36%, v_a = 2.70 m s^{-1}.

The graph of Figure 7a shows a double slope of the drying process. The first slope, lower than the second, is most likely due to the fact that the fabric's electrical conductivity (FEC)was held higher than it should have been until the water in the fabric in excess of its maximum retention capacity was immediately moved away after wetting by gravity (and partly by evaporation). A second reason for this is that part of the thermal power was used to heat the water in the fabric (temperature at the sprinkler = 15 °C),and hence the power was not available for evaporation. The graph of Figure 7b, conversely, presents only one drying slope because the fabric was inserted in the sensor after having been wetted and softly shaken.

The results showed the near-linear correlation with time of the FEC during drying. Furthermore, it is noted that the fabric surface temperature (T_{Ss}) was about constant (mean T_{Ss} = 24.7 °C) during the drying process. It seems that T_{Ss} did not depend on the level of residual water content in the fabric (RWC); this means that the water evaporation rate is almost constant over time. In Chen et al. [11] (Figure 6a), the simulated coat surface by the proposed transient model showed a decreasing trend, and so did the evaporation rate [11]

(Figure 6d). As long as there are liquid continuities across the fabric, evaporation is nearly constant; when continuity is broken (with lower water content), evaporation is also driven by the diffusion of water within the fabric, which makes evaporation slower [19].

Figure 8 shows the good correlation between FEC and RWC; the graph has been obtained in the laboratory by repeating the test of Figure 7a five times, each time starting from the saturation of the fabric (spraying time 20 s), and weighing the fabric upon reaching each 5th of the maximum EC, as in the following procedure.

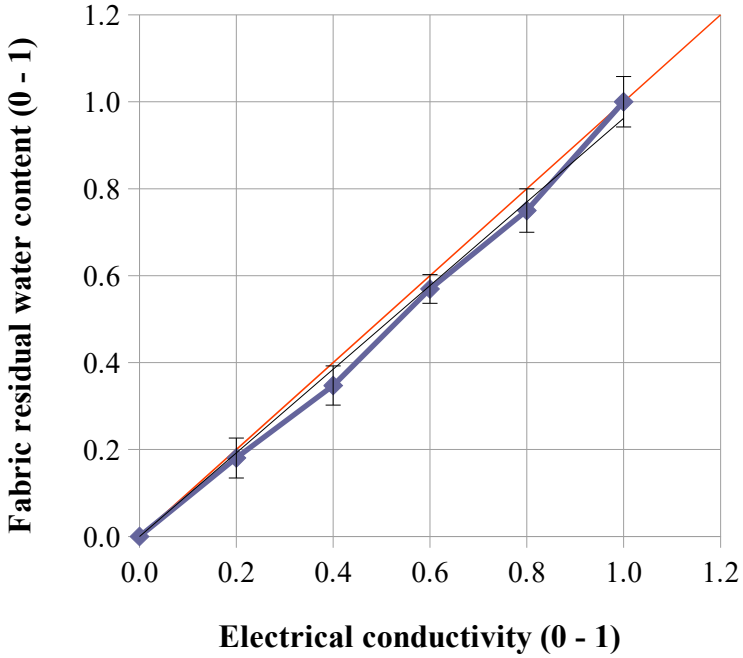

Figure 8. Correlation between fabric residual water content (RWC) and electrical conductivity (FEC), both are unity-based and normalized [0–1].

1. The saturation of the already-assembled fabric with the sensor was attained.
2. Fabric was removed from the sensor and was then weighed.
3. The fabric was re-assembled with the sensor and re-saturated again.
4. The fabric was removed from the sensor when the EC was4/5 of EC_{max}, and was then weighed.
5. Points 3 and 4 were repeated at 3/5 EC_{max}, 2/5 EC_{max},and1/5 EC_{max} (EC_{max} is set at each re-saturation).

Points 1–5 were repeated four times again. At each saturation step, the fabric did not present exactly the same FEC and the same RWC, so the correlation was evaluated considering the normalized values of FEC and RWC (0–1).This procedure was assisted by the control software of the sensor, that gave an alarm at each fifth of saturation. The maximum EC at the end of the spraying was detected when the mean standard deviation (SD) of the EC derivative on time was lower than one, that is, when the following condition was met:

$$\text{if } (SD[d(EC)/dt]?_k/k < 1) \text{ then } EC_{max} = EC \quad (7)$$

Averaging time of the SD was set to k = 10 s.

3.3. Theoretical Cow-Cyl vs. Sensor Thermal Behaviour—Sensitivity Analysis

Figure 9 shows the comparison between the $R_{CS} = Q_c/Q_S$, $R_{CE} = Q_c/Q_{evap}$, and $R_{RE} = Q_s/Q_{evap}$ ratios as ratios between cow-cyl and sensor ($R_{CScow\text{-}cyl}/R_{CSs}$, $R_{CEcow\text{-}cyl}/R_{CEs}$, and $R_{SEcow\text{-}cyl}/R_{SEs}$) by applying the model proposed by Gebremedhin and Wu [10] in a simplified approach. Although the sensor has no similarity with the cow-cyl from a

thermal point of view, some degree of similarity can be considered, especially with higher temperatures and air velocities, as the ratios $R_{cow\text{-}cyl}/R_{sensor}$ becomes closer to unity.

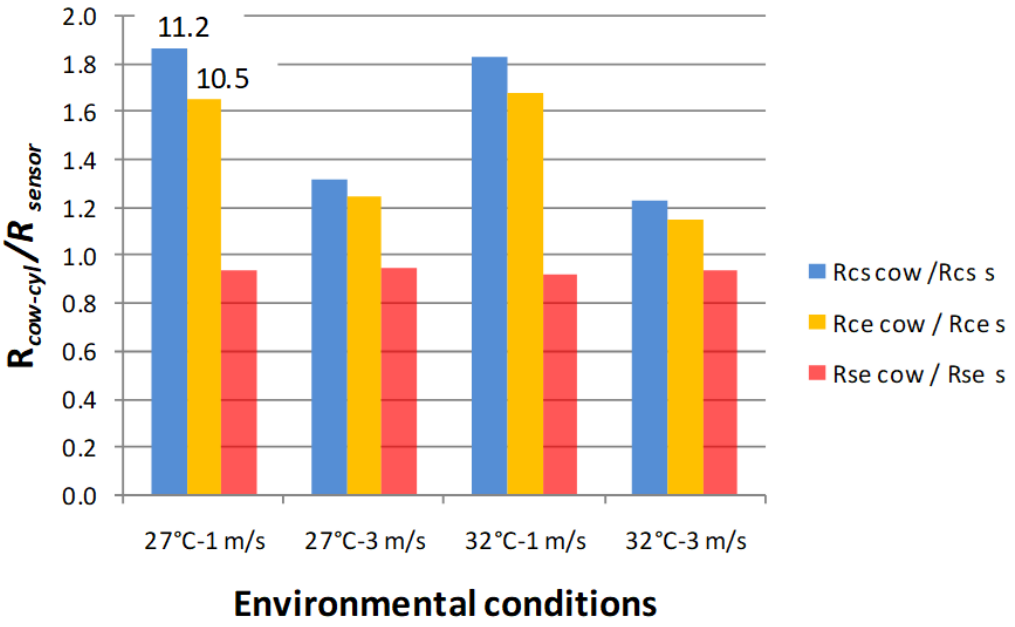

Figure 9. Thermal comparison between the cow as a cylinder (cow-cyl) and sensor ratios ($R_{cow\text{-}cyl}/R_{sensor}$) for the following ratios: $R_{CS} = Q_c/Q_s$, $R_{CE} = Q_c/Q_{evap}$, and $R_{RE} = Q_s/Q_{evap}$ for T_a = 25 and 32 °C, and v_a = 1 and 3 m s^{-1}.

Simulations gave as output $hc_{cow\text{-}cyl}$ local values on average from 9.0 to 16.7 for the cow-cyl, and from 17.1 to 39.5 for the sensor. In Gebremedhin and Wu [10], the average hc for the whole cow-cyl was 8.28 W m^2 K^{-1}. The ratio ($hc_{cow\text{-}cyl}/hc_{Sensor}$) for the corresponding environmental condition ranged from 1.89 to 2.36; so, the higher value of hc_s (1.89–2.36 × $hc_{cow\text{-}cyl}$) due to its lower characteristic length with respect to the cow-cyl, and to the higher Nu number, is partly compensated by a lower value of R_{ins} with respect to R_{tissue} (R_{tissue}/R_{ins} = 0.0585/0.0135 = 4.3). The lowest error was achieved at higher temperatures and air speeds, the conditions most found in the barn in summertime (Figure 9).

Sensitivity analysis revealed a small influence of hc variation on Wa; so, when hc deviated by 70% from the actual value, Wa changed by only 16.9% (Figure 10a), while Ts deviation from the real Ts produced a higher error on Wa. For example, a Ts error of 10% (corresponding to an error of +2.5 °C) from the true value yields an error in Wa evaluation of −22.5% (Figure 10b).

3.4. Field Tests

In Figure 11, two consecutive wetting-drying cycles are reported, as obtained in the experimental barn. In the graph, the unity-based and normalized [0–1] ECs of the fabric and the fur (the latter was measured by the hand EC probe) are shown.

The non-regularity of the EC during drying, with respect to the laboratory test of Figure 7, depends on the varying Ta and RH air condition because it is affected by the sprayer and also by the incoming air from outside. In the trend of EC, the first slope can be distinguished as being lower than the second referred to in the final phase (as described in Section 3.2). The quasi-flat pattern visible in the middle of the EC drying curve (SD label) was due to the reduced fan speed in correspondence to the activation of the sprayer, which, as mentioned above, was closed to allow the complete drying of the fur. The sensor fabric became drier earlier than the fur did, despite the fact that the saturation water content of the fabric was higher than that of the fur (respectively, 273.84 g m^{-2} and 198–230 g m^{-2},

as shown in Table 1). The time the fur became dry is indicated by the EC of the fur (blue markers in Figure 11) becoming zero.

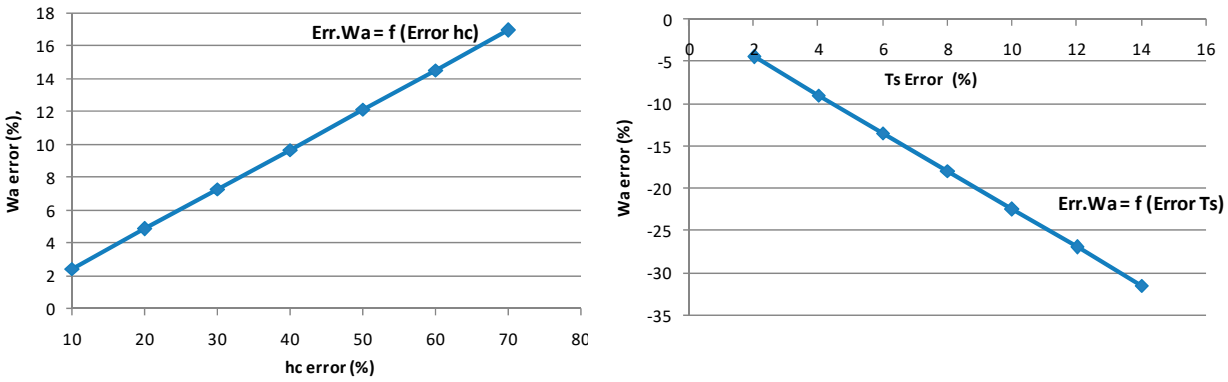

(**a**) (**b**)

Figure 10. Sensitivity analysis. Reference model conditions: Ts = 25 °C, hc = 16 W m^{-2} K^{-1}, and Ta = 32 °C. (**a**) Error Wa $_{cow\text{-}cyl}$ % = f (Error hc $_{cow\text{-}cyl}$ %); and (**b**) Error Wa $_{cow\text{-}cyl}$ % = f (Error Ts $_{cow\text{-}cyl}$, %). With the negative errors of Ts and hc, Wa errors in the graphs must be multiplied by (−1).

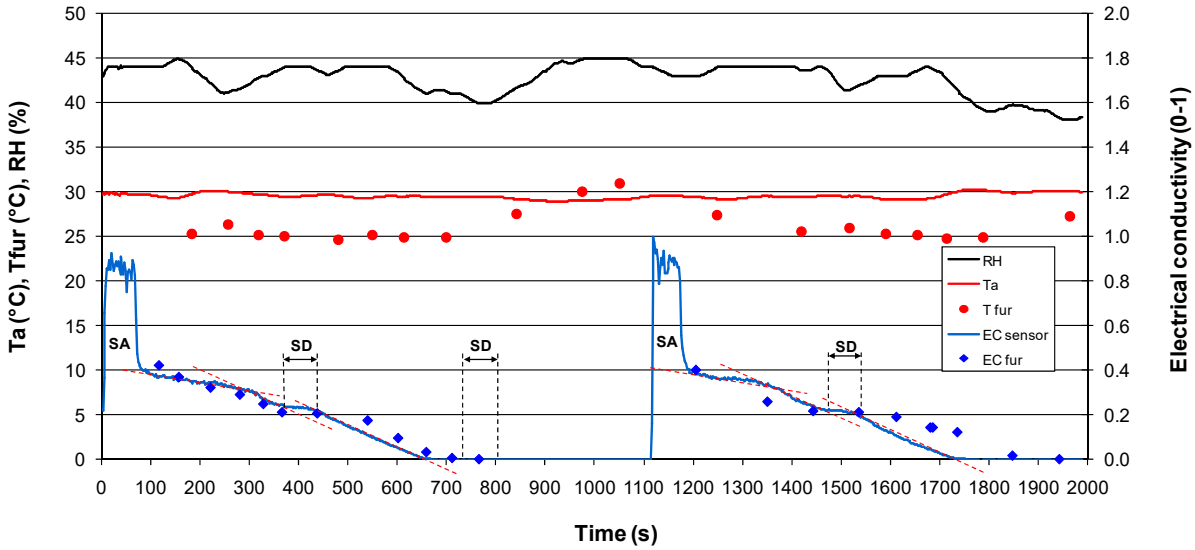

Figure 11. Field test of the drying sensor in the layout of Figure 1: electrical conductivity of the EC fur probe and the sensor fabric, and fur surface temperature by IR temperature meter. SD = Shower disabled, SA = Shower activated: in both cases the fans work at 10% of their maximum speed.

Table 1. Wetness of live cow fur as obtained in April and August (g m^{-2}) by means of the dabbing method described in Section 2.5.

	Min	Max	Mean	DS
April	344.0	481.0	408.2	38.6
August	198.0	230.0	213.4	10.6

In the graph, the fur's IR temperature is almost constant (about 25 °C) during the drying process, showing a similar behavior as the sensor fabric (Figure 7). This fact gives more support to the usability of the sensor in estimating fur drying time.

Applying the model presented in Section 2.9 to adjust the sensor output to estimate the drying time of the fur, we obtain the comparison graph of Figure 12 between the observed

and the predicted drying time (R^2 = 0.789). The error ranges between −11.4% and +14.8%. The comparison of the sensor's response to the predicted values is one of the research outputs of the present manuscript.

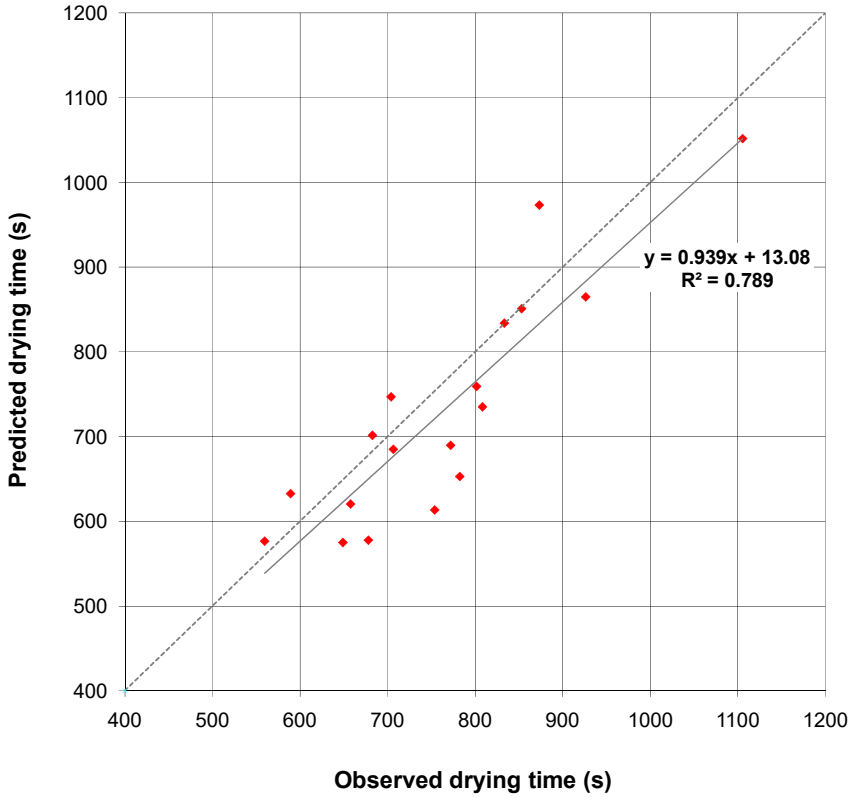

Figure 12. Observed against predicted fur drying time by applying the simplified model of Section 2.9 to the sensor output. The dashed line represents the correct prediction of the drying time.

Chen et al. [11], as already cited, proposed a theoretical transient model and for its validation, only two contexts were considered, recovering the fur water content from a concurrent work. A comparison with the other two authors was done to represent two environmental conditions. In one case, the error ranged from +23% to 30%; in the second case, the error ranged from 2.3% to 37%.

4. Conclusions

Laboratory tests showed good correlation between the EC of the sensor fabric and its residual water content, allowing the estimation of the drying time. Meanwhile, the sensitivity analysis showed that the sensor adequately represented the heat exchanges of the cow.

The error in estimating the fur drying time (between −11.4% and +14.8%) is considered acceptable for the purpose of the sensor presented in the present work, given the high variability of its boundary conditions, even within the same context (i.e., the same barn). For example, the position of the animal at the manger may result in very different levels of ventilation and wetting of the fur; thus, we might have animals that get very wet during spraying, and receive a low-velocity airflow, or vice versa (high/low combinations with respect to wetting/ventilation might also occur).

The use of the sensor in a barn with a sprinkler/fan cooling system can help reduce energy and water consumption. For example, if applied in the barn used for experimentation, with a wetting cycle of 13.8 min (according to the actual drying time of Figure 11), about 52 wetting cycles d^{-1} are foreseen, given a daily operating time of the cooling system of 12 h. If compared to the current barn setting (wetting cycle of 6 min), there

are 120 cycles d^{-1}. So, the use of the sensor in place of the fixed timing will provide a reduction in cycles and thus a reduced water consumption of about 57%.

Finally, we would like to highlight how the presented sensor could not only contribute to greater water and energy efficiency, but also to the improvement of the welfares of dairy cows.

Future Perspectives

From a precision livestock farming (PLF) perspective, as proposed by Chen et al. [11], for the theoretical model, the sensor could also be used both to control the timing of the sprays and to modulate the speed of the fans during drying. For example, if the sensor estimates an excessive evaporation rate, the speed of the fans could be reduced, thus preventing the animals from being over-cooled (as well as reducing the operating costs of the cooling system).

The above perspective will require further experimentation.

Furthermore, as previously anticipated, the sensor could also be used to assess the heat stress level of the cows, keeping in mind that this sensor use will require extensive field experimentation.

Funding: This research received no external funding.

Institutional Review Board Statement: Ethical review and approval were waived for this study because the animals were observed in their daily routine on a commercial livestock farm.

Informed Consent Statement: Not applicable.

Data Availability Statement: The data presented in this study are available on request from the corresponding author.

Conflicts of Interest: The author declares no conflict of interest.

Appendix A

Estimation of $hc_{cow\text{-}cyl}$ and Ts_s from sensor output

This Appendix A explains the approach used to estimate $hc_{cow\text{-}cyl}$ and Ts_s from the sensor output. This Appendix A refers mainly to Incropera et al. [20] (Chapter 6).

Input data:

W_{as} = water evaporation flux obtained from the sensor data (kg m^{-2} s^{-1});

Ta, RH = air temperature (°C) and humidity ratio (%), respectively; and

L = the characteristic linear dimension of the sensor (m).

Output data:

$hc_{cow\text{-}cyl}$ = convective heat transfer of the cow-cyl (W m^{-2} K^{-1});

Ts_s = surface;

Legend

NA_s = molar flux of water vapour (kmol m^{-2} s^{-1});

CAs = molar concentration of the surface of the sensor (kmol m^{-3});

CAa = molar concentration of the undisturbed air (kmol m^{-3});

D_{AB} = mass diffusion coefficient of water vapour in air (m^2 s^{-1});

hm_s = convective mass transfer coefficient of the sensor (m s^{-1});

hc_s = convective heat transfer of the sensor (W m^{-2} K^{-1});

Sh = Sherwood number;

v_{as} = undisturbed air velocity (m s^{-1});

MW_w = water molar weight (kg $kmol^{-1}$);

R_{ins} = resistance of the insulation layer of the sensor (m^2 K W^{-1});

Ts_s = surface temperature of the sensor (°C);

Sc = Schmidt number;

Pr = Prandtl number;

ν = kinematic viscosity (m^2 s^{-1});

D = cow-cyl diameter = 0.8 m; and

k = air thermal conductivity (W m^{-1} K^{-1}).

By incrementing T_s at each iteration step (starting from $T_s = Ta - 10$) we check until the following condition is reached:

$$Q_s = Q_c + Q_{evap} \quad (A1)$$

That is:

$$(T_{Bs} - Ts_s)/R_{ins} = hc_s(Ts_s - T_a) + W_{as} \cdot J \quad (A2)$$

Starting from the evaporated water from the sensor Wa_s (kg m^{-2} s^{-1}), obtained as the slope of EC(t) (Equation (4)), we obtain the molar flux NA as:

$$NA_s = W_{as}/MW_w \quad (A3)$$

Which is [20] (Chapter 6):

$$NA_s = hm_s(CAs - CAa) \quad (A4)$$

The convective mass transfer coefficient hm_s is calculated as:

$$hm_s = NA_s/(CAs - CAa) \quad (A5)$$

Which is:

$$hm_s = Sh_s \cdot D_{AB}/L \quad (A6)$$

$$Sh_s = hm_s\ L/D_{AB} \quad (A7)$$

Considering the following heat-mass transfer analogy relation [14,22] valid for turbulent or laminar flow:

$$Sh/Nu = (Sc/Pr)^{1/3} \quad (A8)$$

We can calculate the Nu number of the sensor from Sh_{sensor}:

$$Nu_s = Sh_s/(Sc/Pr)^{1/3} \quad (A9)$$

Then:

$$hc_s = Nu_s\ k/L \quad (A10)$$

From the Nu_{sensor}, backwards from Abd-Rabbo et al. [21] (Figure 10),we can find the Re number for a square cube, and consequently va_{sensor}:

$$v_{as} = Re_s\ \nu/L \quad (A11)$$

From this, we can calculate $Nu_{cow\text{-}cyl}$ local from [20] (Figure 7.9) and $hc_{cow\text{-}cyl}$ local as:

$$hc_{cow\text{-}cyl} = Nu_{\ cow\text{-}cyl}\ k/D \quad (A12)$$

References

1. Ji, B.; Banhazi, T.; Perano, K.; Ghahramani, A.; Bowtell, L.; Wang, C.; Li, B. A review of measuring, assessing and mitigating heat stress in dairy cattle. *Biosyst. Eng.* **2020**, *199*, 4–26. [CrossRef]
2. Fournel, S.; Ouellet, V.; Charbonneau, É. Practices for Alleviating Heat Stress of Dairy Cows in Humid Continental Climates: A Literature Review. *Animals* **2017**, *7*, 37. [CrossRef]
3. Bleizgys, R.; Česna, J.; Kukharets, S.; Medvedskyi, O.; Strelkauskaitė-Buivydienė, I.; Knoknerienė, I. Adiabatic Cooling System Working Process Investigation. *Processes* **2023**, *11*, 767. [CrossRef]
4. Igono, M.; Johnson, H.; Steevens, B.; Krause, G.; Shanklin, M. Physiological, productive, and economic benefits of shade, spray, and fan system versus shade for holstein cows during summer heat. *J. Dairy Sci.* **1987**, *70*, 1069–1079. [CrossRef]
5. Keister, Z.; Moss, K.; Zhang, H.; Teegerstrom, T.; Edling, R.; Collier, R.; Ax, R. Physiological responses in thermal stressed Jersey cows subjected to different management strategies. *J. Dairy Sci.* **2002**, *85*, 3217–3224. [CrossRef]

6. Collier, R.J.; Dahl, G.E.; VanBaale, M.J. Major advances associated with environmental effects on dairy cattle. *J. Dairy Sci.* **2006**, *89*, 1244–1253. [CrossRef]
7. Neves, S.F.; Silva, M.C.F.; Miranda, J.M.; Stilwell, G.; Cortez, P.P. Predictive Models of Dairy Cow Thermal State: A Review from a Technological Perspective. *Vet. Sci.* **2022**, *9*, 416. [CrossRef]
8. Shu, H.; Li, Y.; Bindelle, J.; Jin, Z.; Fang, T.; Xing, M.; Guo, L.; Wang, W. Predicting physiological responses of dairy cows using comprehensive variables. *Comput. Electron. Agric.* **2023**, *207*, 107752. [CrossRef]
9. Kimmel, E.; Arkin, H.; Broday, D.; Berman, A. A model of evaporative cooling in a wetted hide. *J. Agric. Eng. Res.* **1991**, *49*, 227–241. [CrossRef]
10. Gebremedhin, K.; Wu, B. A model of evaporative cooling of wet skin surface and Fur layer. *J. Therm. Biol.* **2001**, *26*, 537–545. [CrossRef]
11. Chen, E.; Narayanan, V.; Pistochini, T.; Rasouli, E. Transient simultaneous heat and mass transfer model to estimate drying time in a wetted fur of a cow. *Biosyst. Eng.* **2020**, *195*, 116–135. [CrossRef]
12. Arkin, H.; Kimmel, E.; Berman, A.; Broday, D. Heat transfer properties of dry and wet furs of dairy cows. *Trans. ASAE* **1991**, *34*, 2550–2558. [CrossRef]
13. Macavoray, A.; Afzal Rashid, M.; Rahman, H.; Qamer Shahid, M. On-Farm Water Use Efficiency: Impact of Sprinkler Cycle and Flow Rate to Cool Holstein Cows during Semi-Arid Summer. *Sustainability* **2023**, *15*, 3774. [CrossRef]
14. Tresoldi, G.; Schütz, K.E.; Tucker, C. Cooling cows with sprinklers: Spray duration affects physiological responses to heat load. *J. Dairy Sci.* **2018**, *101*, 4412–4423. [CrossRef]
15. Chen, J.; Schutz, K.E.; Tucker, C.B. Cooling cows efficiently with sprinklers: Physiological responses to water spray. *J. Dairy Sci.* **2015**, *98*, 6925–6938. [CrossRef]
16. Means, S.L.; Bucklin, R.A.; Nordstedt, D.K.; Beede, D.R.; Bray, C.J.; Wilcox, W.; Sanchez, W.K. Water application rates fora sprinkler and fan system in hot, humid climates. *Appl. Eng. Agric.* **1992**, *8*, 375–379. [CrossRef]
17. Ding, T.; Sun, B.; Shi, Z.; Li, B. Optimizing Water Droplet Diameter of Spray Cooling for Dairy Cow in Summer Based on Enthalpy Difference Theory. *Energies* **2019**, *12*, 3637. [CrossRef]
18. Tresoldi, G.; Schütz, K.E.; Tucker, C.B. Cooling cows with sprinklers: Timing strategy affects physiological responses to heat load. *J. Dairy Sci.* **2018**, *101*, 11237–11246. [CrossRef] [PubMed]
19. Gonçalves, T.D.; Brito, V.; Vidigal, F.; Matias, L.; Faria, P. Evaporation from Porous Building Materials and Its Cooling Potential. *J. Mater. Civ. Eng.* **2015**, *27*, 04014222. [CrossRef]
20. Incropera, F.P.; DeWitt, D.P.; Bergman, T.L.; Lavine, A.S. *Fundamentals of Heat and Mass Transfer*, 6th ed.; John Wiley & Sons, Inc.: Hoboken, NJ, USA, 2007; Chapters 6, 7, 9.
21. Abd-Rabbo, M.A.; Berbish, N.S.; Mohammad, M.A.; Mandour, M.M. Forced convectio heat transfer from three dimensional bodies in cross-flow. *Eng. Res. J.* **2013**, *137*, M1–M19.
22. Goldstein, R.J.; Yoos, S.Y.; Chung, M.K. Convective mass transfer from a square cylinder and its base plate. *Int. J. Heat Mass Transfer.* **1990**, *33*, 9–18. [CrossRef]